[5] Swithenbank, J. and Harris, D., "Intentional Combustion Oscillations in Propulsion Systems," Rept. HIC 45, 1956, University of Sheffield, England.

[6] Flandro, G. A., "Rotating Flows in Acoustically Unstable Rocket Motors," Ph.D. thesis, 1967, California Institute of Technology, Pasadena, Calif.

[7] Hribar, A. E., "The Effect of a Transverse Resonant Acoustic Field Upon Viscous Fluids in Cylindrical Enclosures," Ph.D. thesis, 1969, Purdue Univ., Lafayette, Ind.

[8] Hribar, A. E. and Purdy, K. R., "On the Interaction of Intense Acoustic Fields and Viscous Fluid Flow," *Transactions of the ASME, Ser. D: Journal of Basic Engineering*, Vol. 91, No. 1, March 1969, pp. 74–80.

[9] Culick, F. E. C., "Acoustic Oscillations in Solid Propellant Rocket Chambers," *Astronautica Acta*, Vol. 12, No. 2, March-April 1966, pp. 113–136.

[10] Van Dyke, M., *Perturbation Methods in Fluid Mechanics*, Academic Press, New York, 1964.

[11] Stuart, J. T., "Unsteady Boundary Layer," *Laminar Boundary Layer, Part VII*, Clarendon Press, Oxford, 1963, pp. 347–408.

JUNE 1971 AIAA JOURNAL VOL. 9, NO. 6

Two-Phase Seeding in Low-Density Plasma Flow

HWACHII LIEN* AND GERALD STEPAKOFF†
Avco Systems Division, Wilmington, Mass.

Numerical solutions of a typical boundary-layer seeding problem at low pressure are presented to demonstrate the important roles played by the interaction of heterogeneous fluid flow and chemical processes. A physicochemical model is developed for the investigation of the coupling of heterogeneous vaporization kinetics in a rarefied atmosphere, with the distribution of ionic and neutral species and homogeneous gas phase chemistry. It is found that the seeding effectiveness, as indicated by the evaporation efficiency and the degree of ionization for a given injection mass flow rate, is essentially controlled by the initial droplet size, the velocity and the direction of injection, kinetics of vaporization, and chemical processes.

1. Introduction

ENHANCEMENT of flowfield electron densities by seeding has been an intensive area of study in recent years. The first investigations were concerned with chemical kinetics of combustion processes and these were followed by practical extensions to MHD, ion propulsion, and reentry plasma seeding applications.‡ In order to accomplish effective seeding in these processes, it is necessary to carefully select the seedant material and also to investigate the effects of fluid dynamic and chemical kinetic coupling of the injectant with the plasma stream. The following study was made to provide some basic information concerning this coupling problem in relation to the boundary-layer seeding application.

The problem under investigation is the injection of aqueous solutions of alkali salt through a nozzle into a low-density, high-temperature boundary-layer plasma flow for the purpose of enhancing the electron density level. The alkali salts are considered good seedants because they provide a convenient source of alkali metal vapor when subjected to a high-temperature environment. The low ionization potential of the metal vapor results in increased ionization in the gas phase.

The coupling of the heterogeneous vaporization and gas phase ionization with the rarefied flowfield have been previously studied by several investigators. For example, the analytical formulation of predicting the mean drop size from a liquid jet has been proposed by Adelberg[3] following the modified approach of Mayer.[4] Extensive analyses for heterogeneous flow problems including such studies as condensation, two-phase nozzle flow and effect of aerodynamics on heterogeneous flow, can be found in two symposium proceedings[5,6] and in the series of the Proceedings of the International Symposium on Combustion. Although excellent detailed discussions on many basic research topics dealing with two-phase flow are given in these Proceedings, none deals with a specific application of boundary-layer seeding by injection of an aqueous solution under high altitude re-entry conditions. A published study more closely related to the problem studied in this paper is that of Edelman and Rosenbaum.[7] However, the solution obtained in Ref. 7 is for an axisymmetric chemically frozen jet with solid-vapor phase equilibrium, as compared to the present approach where the nonequilibrium chemical reactions and distillation process of the seedants are considered. Moreover, the effect of the droplet distribution of the injected fluid in various sizes over the entire flowfield is included in the present analysis. It is demonstrated that this distribution is an important factor controlling the interaction between the droplets and the gas flow.

2. Formulation of the Problem

On recognizing the very complex nature of the present problem, the introduction of certain assumptions becomes necessary for making the analysis feasible. The validity of these assumptions, under certain given conditions, are here discussed. 1) The size and the number density of the injectant droplets are so small that the disturbances of the boundary-layer flow due to seedant injection are neglected except for the effect of nonequilibrium chemical reactions. 2) In connection with the preceding statement, droplet-droplet interaction is neglected. 3) For small droplet size considered in the present problem, the conduction and convection within the droplet is neglected. Consequently, the temperature within the droplet is assumed uniform.

In general, the simplified approach of the present analysis is to treat the coupling of the heterogeneous flow unilaterally rather than simultaneously. That is, the vaporization of the

Received February 10, 1970; revision received October 2, 1970. A portion of the material in this paper was presented at the AIAA Fluid and Plasma Dynamics Conference at Los Angeles, Calif., June 24–26, 1968. The authors wish to express their appreciation to A. Pallone for helpful discussions.

* Assistant Department Manager, Observables and Counter Measures; presently Visiting Professor, National Taiwan University.

† Group Leader, Applied Technology Department. Member AIAA.

‡ Numerous papers have been published in a series of the Proceedings of International Symposium on Combustion. Many more articles can be found in other related publications, such as Refs. 1 and 2.

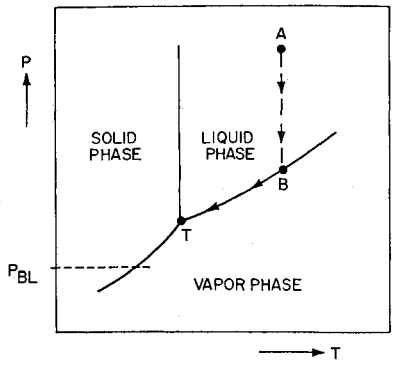

Fig. 1 Phase diagram for H_2O.

droplet is first analysed based on the local velocity and temperature field of the undisturbed boundary-layer flow. The mass transfer from the droplets computed as a function of size and trajectory is integrated over the entire distribution space and then imposed on the gas-phase boundary-layer calculation governed by the species conservation equations. Since the primary objective of this study is to assess the over-all effectiveness of the injection seeding in the boundary-layer flow at high altitudes, the mass transfer and its associated chemical effects are analyzed in more detail than the momentum and the energy transfer. As far as the ionization level in the flowfield is concerned, the neglect of bilateral coupling in the momentum and the energy transfer is a second-order effect under the conditions stated above.

3. Aerothermochemistry of Seeding

To produce electrons by the gas-phase ionization reactions of the injected seedant solution, the solvent must first be distilled from the solution droplets and the remaining salt crystals must vaporize. Therefore, the first step in the analysis is the study of transfer processes associated with the droplet evaporation.

Considering the mass and energy conservation of a droplet, the governing equations for an open system across the droplet surface are,

$$\hat{m} + \bar{m} = \text{const} = m_0 \tag{1}$$

$$d(\hat{m}\hat{h}) + \bar{h}d\bar{m} + dq = 0 \tag{2}$$

where the symbols ($\hat{}$) and ($\bar{}$) represent liquid and gas phases, respectively.

The first term in Eq. (2) represents the change in total energy of the liquid droplet, whereas the second and third terms represent, respectively, the convected energy leaving the droplet due to the evaporated mass and the heat transfer from the droplet to the environment. The effect of surface energy is neglected. Since the total enthalpy of the fluid is

$$\bar{h} = \hat{h} + (\Delta h)_v \tag{3}$$

where $(\Delta h)_v$ denotes the latent heat, the combination of Eqs. (1–3) yields,

$$(\Delta h)_v dm + (m_0 - \bar{m})C_p dT + dq = 0 \tag{4}$$

In order to solve Eq. (4) for the vaporized mass m_v, the relation expressing dq in terms of dT must be found with respect to the flowfield environment. This heat-transfer equation for determining the dq across the droplet surface must be coupled with Eq. (4), and the resulting set of simultaneous linear differential equations must be integrated along the droplet trajectory to find the mass of vaporization m_v. The preceding method of solution is further complicated by the fact that the limit of integration for solving these differential equations is not a predetermined quantity. It depends on the residence time of the droplet in the flow, which, in turn, depends on the size of the particle and the magnitude and direction of its velocity.

An approximate solution to Eq. (4) is obtained by integrating the equation in two steps. The first step is a quasi-adiabatic step with $dq = 0$ and corresponds to the initial rapid expansion period. The second step is a subsequent exposure to hot environment period in which the system departs from equilibrium conditions.

With reference to the phase diagram for an aqueous solution of sodium hydroxide (NaOH) represented by Fig. 1, the vapor pressure is assumed to reach the environmental boundary-layer pressure after expansion through the nozzle. As the droplets suddenly expand into the region of reduced pressure during the initial atomization period (from A to B in Fig. 1), the temperature of the droplets remains approximately constant. This can be seen from the following argument. Since $dQ = du + pdv = 0$ and $pdv \simeq 0$ for a liquid, then $du = C_v dT \simeq 0$ or $T \simeq$ const.

As long as the liquid is in equilibrium with the vapor, the thermodynamic state will then change from B moving toward the triple point along the saturation line. By means of an analysis similar to that of Ref. 8, the time required for cooling a water droplet of 30 μ diam from 80°F to the triple point temperature and the time required for the droplet to freeze at the triple point under the adiabatic condition are found to be approximately 1.6 and 18 msec, respectively. Based on the result of Ref. 8 that the freezing at the triple point is a much slower process than the cooling of the droplet from its initial liquid temperature to the triple point, and the estimation that the adiabatic process lasts no more than a few milliseconds before heat transfer starts to be influential, an approximate initial rapid expansion period with adiabatic cooling is assumed to proceed to the neighborhood of the triple point. Thereafter, the droplet vaporization will be strongly controlled by the heat transfer from the hot boundary-layer environment. Strictly speaking, the final state for the adiabatic process will not be at the triple point conditions. Depending on the onset of the heat transfer, the droplet will depart from equilibrium slightly before or after reaching the triple point. In any case, the error induced is quite small as far as the estimate on the amount of vaporization is concerned.

For the initial adiabatic process, the mass of vaporization can be evaluated by integrating Eq. (4) with $dq = 0$. This yields an implicit formula,

$$m_v(\Delta h)_v = \int_{T_T}^{T_A} (m_0 - m_v)C_p dT \tag{5}$$

which can be solved by an iterative procedure with small integration increments. In a finite difference form, Eq. (5) becomes

$$m_v = \sum_i \Delta m_i = \sum_i \frac{(m_0 - m_v)_i(\Delta h)_i}{(\Delta h)_v} \tag{6}$$

where the value for the term $(m_0 - m_v)_i$ is computed using the value of m_v taken at the previous summation limit $i - 1$. With sufficiently small finite-difference intervals, the error can be minimized in converting the implicit expression, Eq. (5), to the explicit form, Eq. (6). For T_A at room temperature and T_T at triple point temperature, the estimate by Eq. (6) indicates that only a small percentage of the droplet mass is vaporized by the initial adiabatic expansion process. The droplet size is hardly changed during this process since the reduction in droplet diameter D is proportional to the cube root of m_v.

As already mentioned, the initial rapid expansion is followed by another stage of the vaporization process during which the droplets experience high heat-transfer rates from the hot flowfield environment. The process is no longer adiabatic, and the mass of vaporization must be calculated from the coupled mass, momentum, and energy transfer equations for the heterogeneous system. It is noted that this stage of vaporization due to heat transfer produces the major portion of the

seedant vapor as compared with the amount produced during the adiabatic expansion.

As a first approximation, it is assumed that the temperature within the droplet is uniform (thus ignoring the heat conduction to the droplet) and that the mass diffusion due to the gradient in the chemical potential is large enough to carry away the mass as it is vaporized. A simple heat balance equation for each droplet then yields a relation,

$$(dm_v/dt)(\Delta h)_v = A(\mathbf{s})\cdot\bar{h}(\mathbf{s})[T_g(\mathbf{s}) - T_T] \tag{7}$$

where A is the surface area of the droplet, $\bar{h}$ is the convective heat-transfer coefficient, and the subscript g refers to the gas phase. Since the droplets travel in the nonuniform boundary-layer region following the curvilinear path $\mathbf{s}$, Eq. (7) must be coupled with the trajectory equation to define the variation of environmental temperature T_g and convective heat-transfer coefficient $\bar{h}$ along the path. The coupling with a trajectory equation and the method of solution for the present problem will be discussed in detail later. Introducing the relations

$$A = \pi D^2 \quad \text{and} \quad m_v = (\pi\rho/6)(D_0^3 - D^3)$$

and expressing $\bar{h}$ in terms of the Nusselt number $\langle Nu\rangle = \bar{h}D/\kappa_g$; Equation (2) can then be rewritten in the form

$$-(\pi\rho D^2/2)(dD/dt)(\Delta h)_v = \pi(D^2\langle Nu\rangle/D)\kappa_g(T_g - T_T)$$

or

$$DdD/dt = -2\kappa_g\langle Nu\rangle(T_g - T_T)/\rho(\Delta h)_v \tag{8}$$

where κ_g is the thermal conductivity of the gas.

The variation of T_g along the droplet path, which is required in order to solve Eq. (8), can be obtained by a proper mapping of the droplet trajectory with the boundary-layer temperature variation. Corrections for the vaporization and the chemical reactions are carried out by an iterative calculation of the temperature distribution. Note that it is only those droplets with the residence time longer than the water vaporization time which contribute to effective seeding, since the solvent must distill off from the electrolyte solution before the salt can be vaporized.

In order to calculate the particle residence time, the velocity and the distance traveled by the droplet must be known. This information is obtained from the solution of the following vector equation of motion:

$$m\,d\mathbf{V}/dt = \frac{-C_D\rho_g(\mathbf{V} - \mathbf{V}_g)|\mathbf{V} - \mathbf{V}_g|}{2}\cdot\frac{\pi D^2}{4} \tag{9}$$

with

$$d\mathbf{s}/dt = \mathbf{V} \tag{10}$$

Equations (8–10) are the first-order coupled ordinary differential equations for the complete solution of the vaporization problem.

The first step in solving the preceding equations is to specify the environmental condition $\mathbf{V}_g$ and $\mathbf{T}_g$ in the boundary-layer region. This information is readily available from published data such as Refs. 9 and 10. Again, it is emphasized that the mass flow rate of seedant solution being injected into the boundary layer is low enough so that the perturbation of the velocity and enthalpy profiles in the boundary layer can be neglected.

The process involving the surface heat transfer with evaporation is very complex and a precise analysis should follow the approach described in Ref. 11. However, by assuming the value of Lewis number to be nearly equal to one, Eq. (8) can be used in the present analysis to estimate the over-all nature of the droplet vaporization, rather than the exact details. In order to solve Eq. (8), it is necessary to know the value of the heat-transfer coefficient. In a rarefied flowfield, the heat-transfer coefficient is decreased below its continuum value. This is primarily due to the imperfect accommodation and temperature slip condition which induces an effective thermal contact resistance at the surface. Over-all average heat-transfer coefficients for spheres in a rarefied subsonic air stream are available from the correlation of theoretical and experimental results as[12]

$$\langle Nu\rangle = \langle Nu_0\rangle/[1 + 3.42\,M\langle Nu_0\rangle/Re\cdot Pr] \tag{11}$$

where $P_r = \mu/\kappa C_p$ = Prandtl number, $R_e = D(V_g - V)\rho_g/\mu$ = Reynolds number, and M = Mach number of the flow with respect to the droplet. The quantity $\langle Nu_0\rangle$ is the average Nusselt number for continuum flow, which has been evaluated elsewhere. For example, an expression such as Drake's formula[13]

$$\langle Nu\rangle_0 = 2 + 0.459(Re)^{0.55}(Pr)^{0.33} \tag{12}$$

may be used without loss of generality here. The drag coefficient needed to solve Eq. (9) for the transition region flow and the Stokes flow is obtained from available published data and is applied here in tabulated form as a function of Mach number and Reynolds number. Reference 14 summarizes the recent treatment on the subject, and presents extensive correlations of C_D as functions of R_e and M.

Since the seedant vapor does not form until the vaporization of the water is completed, the amount of seedant vapor produced in the flow is limited by the rate of this distillation process. Knowing the concentration of the alkali salt in water and the initial droplet size, the time history of the distillation process for each droplet can be studied by solving Eqs. (8–10) with the value of $(\Delta h)_v$ taken as the heat of vaporization of water. Following the completion of the distillation process, the similar computation with the value of $(\Delta h)_v$ taken as the heat of sublimation§ of the seedant is continued along the droplet trajectory to determine the rate of seedant vaporization. Next, these results along each droplet are summed up for all trajectories and then redistributed within a local mixing volume with the boundary-layer air flow. This numerical mapping scheme for computing the mass fractions of air, water vapor, and seedant vapor within each small finite difference volume cell is extended over the entire flowfield domain of interest.

After the properties of the mixture in the flowfield are specified, the chemical processes can be studied by a nonequilibrium stream tube computer program. Specifically, the boundary-layer equations without injection with proper momentum and energy diffusion are solved first[9] to provide a velocity and enthalpy profile along the stream tube for the solution of the species conservation equations,

$$\rho u\,\partial c_i/\partial x = \dot{w}_i]_{\text{chem}} + \dot{w}_i]_{\text{vap}} \tag{13}$$

where

$$\dot{w}_i]_{\text{chem}} = (d/dt)(\rho c_i) \quad \text{and} \tag{14a}$$

$$\frac{d(\rho c_i)}{dt} = M_i\sum_k\left[(\nu_i'' - \nu_i')k_f\prod_j\left(\frac{\rho c_j}{M_j}\right)^{\nu_j'} + (\nu_i' - \nu_i'')k_b\prod_j\left(\frac{\rho c_j}{M_j}\right)^{\nu_j''}\right]_k \tag{14b}$$

Equation (14) is the general law of mass action in a form consistent with Ref. 15 and represents the rate of chemical production of species i. The quantities ν_i' and ν_i'' represent the stoichiometric coefficients, c_j the mass fraction of the jth species, M_i the molecular weight of species i, with k_f and k_b denoting the reaction rate constants for the forward and backward reaction involving c_i. The summation over K accounts for the entire contribution to the production (or depletion) of the species i from all chemical reactions involving c_i in the system.

§ JANAF Thermochemical Tables, Dow Chemical Co., Midland, Mich.

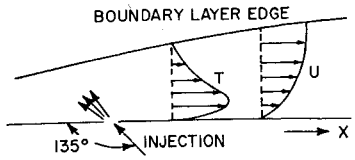

Fig. 2 Boundary layer with injection.

The term $\dot{w}_i]_{\text{vap}}$ in Eq. (13) represents the source term due to vaporization along the stream tube under a condition that

$$\dot{w}_i]_{\text{vap}} = 0 \text{ for } i \neq l, m \tag{15}$$

where the indices l and m correspond to seedant and water. A numerical example of the calculation of $\dot{w}_l]_{\text{vap}}$ and $\dot{w}_m]_{\text{vap}}$ by a finite-difference scheme is demonstrated in the following section. Since none of the droplet trajectories are in parallel to the stream tube, a certain extent of the diffusion effects involving the seedant and the water vapors is included in the stream tube computation by the cross coupling of the droplet trajectories with the stream tubes. Although the effects of diffusion of other chemical species ($i \neq l, m$) is not included in Eq. (13), it is estimated that the neglect of the species diffusion across the stream tubes can introduce an error factor of only two to three[16] in the computation of the electron density distribution. In keeping with other approximations made in this work, the stream tube approach is considered appropriate here for investigating the gross effects of the seeding and for determining the general trends of the various parameters.

4. Chemical Kinetics

The injection of aqueous solutions of sodium hydroxide (NaOH) as a seedant is considered in the present study for the following practical reason. Injection of a solution is better suited for introducing a controlled amount of seedant into the plasma, and is easier to handle than powdered NaOH, thereby assuring the reliability and simplicity of the hardware system used for the injection process.

The rate constants used in the present calculations are taken from several sources. Clean air reactions are based on compilations of Wray[17] and Sutton.[18] The thermal dissociation rate of NaOH was scaled to that for water with the activation energy equal to the NaOH bond energy.[19] The major ionization processes for the seeded plasma were assumed to be thermal ionization of sodium atoms with equivalent efficiencies for all collision partners,[20] chemi-ionization of water[21] to form H_3O^+, ionic recombination, heavy ion neutralization and electron attachment. It is noted that two body dissociative electron attachment reactions to HOH and NaOH are included in the chemical model in addition to the slower three-body collision attachment to species such as the OH radical.[20] The activation energy for these processes was estimated as the difference between the (M-OH) bond energy and the electron affinity of OH. For the latter quantity, the result of Branscomb, 1.8 ev, was used.[22] Ion recombination processes included three-body recombination of electrons with atomic sodium ions, dissociative recombination and charge transfer processes.

In certain ionic reactions where the availability of experimental data is limited, theoretical models were used to estimate the cross sections of rate constants. These theoretical models include the ionic recombination theory of Landon and Keck,[23] charge transfer theory of Gioumousis and Stevenson,[24] two-body neutralization theory of Johnston,[25] and dissociative recombination model of Hansen[26] for the reaction between $NO^+ + e^-$. Table 1 summarizes the set of chemical reactions and corresponding rate constants which have been identified as the dominant processes in the seeding chemistry. (Reverse rate constants not shown in Table 1 were computed from the equilibrium constants.)

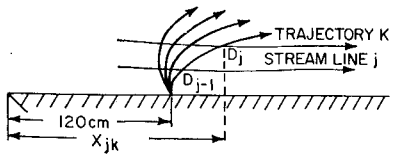

Fig. 3 Droplet trajectories and stream lines.

5. Numerical Computation

To illustrate the method of solution, a boundary-layer seeding over a flat plate was chosen as a representative flowfield environment. The injected mass flow rates were taken to be 0.1 and 1.0 g/sec with the injection angle of 135°. Figure 2 shows the injection geometry. The mean droplet size (after atomization through impinging nozzles) and the injection velocity are estimated from experimental data to be 30 μ and 5 m/sec., respectively. The freestream velocity is 6000 m/sec, and the pressure over the boundary layer is 2×10^{-3} atm.

As previously discussed, the local value of $\langle Nu \rangle$ must be evaluated by Eq. (11) before the integration of Eqs. (8–10) can be performed. Since Eq. (11) is obtained from the correlations of subsonic data, the validity of its application under a given flowfield condition must be first examined. For the case studied here, the relative flows over the droplets are found to be subsonic (by computing the actual trajectory for each droplet) throughout the evaporation period.

Through atomization and jet expansion processes, the seedant flow at the nozzle exit will break up to form streams of droplets with different diameters and different injection angles. The trajectories for the various classes of droplets are sketched in Fig. 3. The water and NaOH vaporization from these trajectories consist of $\dot{w}_{l,m_{\text{vap}}}$ for each stream tube (strictly speaking, stream lamina in the two-dimensional flow). For example, the contribution to the stream tube j at X_{jk} from the droplet K, as shown in Fig. 3, is approximated as

$$(\dot{w}_{l,m}]_{\text{vap}})_{jk} = (\pi\rho/6)(D^3_{j-1} - D^3_j)(\dot{n}_k) \tag{16}$$

where $\dot{n}_k$ is the total number of particles flowing along the trajectory K in a unit time [see Eq. (21)]. It follows that the total contribution to the stream tube j from all the trajectories can be calculated from this finite-difference scheme along the stream tube as

$$(\dot{w}_{l,m}]_{\text{vap}})_j = \sum_k (\dot{w}_{l,m}]_{\text{vap}})_{jk} \tag{17}$$

The numerical value for $\dot{n}_k$ which is needed in the computations of Eqs. (16) and (17) can be determined from the mass continuity equation for the injection as follows. First, the

Table 1 Main chemical reactions and rate constants for electron and ion chemistry of seeding

Reaction	Rate constant[a], $cm^3\ mole^{-1}\ sec^{-1}$ A	B	C	Reference
Air reactions				
$e^- + NO^+ = N + O$	4×10^{18}	$-\frac{1}{2}$	0	18
$O_2^- + O_2 = O_2 + O_2 + e^-$	5.4×10^9	1.5	9913	18
$O_2^- + N_2 = O_2 + N_2 + e^-$	5.4×10^9	1.5	9913	18
Alkal-metal reactions				
$NaOH + M = Na + OH + M$ (N_2), (O_2), (H_2O)	3.2×10^{20}	−1	38752	19
$Na + H_2O = NaOH + H$	1.8×10^{13}	0	22144	19
$Na + M = Na^+ + e^- + M$	1.6×10^{16}	$\frac{1}{2}$	59134	20
$Na + O_2 = Na^+ + O_2^-$	1.8×10^{15}	0	54172	19
$Na + OH = Na^+ + OH^-$	1.8×10^{15}	0	38314	19
$Na + O = Na^+ + O^-$	1.8×10^{15}	0	42597	19
$Na + NO^+ = Na^+ + NO$	3×10^{12}	$-\frac{1}{2}$	0	19
$NaOH + e^- = Na + OH^-$	6×10^{13}	0	17800	Estimated
Water reactions				
$HOH + M = H + OH + M$	3.2×10^{20}	−1	59403	19
$OH + e^- + M = OH^- + M$	1.1×10^{18}	0	0	19
$HOH + H = H_3O^+ + e^-$	6×10^6	1.6	70000	19
$HOH + e^- = H + OH^-$	6×10^{13}	0	38300	Estimated

[a] $k = AT^B \exp(-C/T)$.

rate of the total mass flow is expressed in terms of the total number $\dot{n}_q$ of particles having a diameter of the class D_q as

$$\dot{M}_{\text{inj}} = \sum_q m_q \dot{n}_q = (\pi\rho/6) \sum_q D^3{}_q \dot{n}_q \qquad (18)$$

Introducing a Gaussian distribution in size D_q through the nozzle as indicated in Fig. 4,

$$\dot{n}_q = \dot{n}_0 \exp\{-\beta(D_q - \bar{D})^2\} \qquad (19)$$

where β is a characteristic constant for the distribution function and $\bar{D}$ is the mean diameter; the value of the total number $\dot{n}_0$ for the $\bar{D}$ diameter class can be calculated by the combination of Eqs. (18) and (19), i.e.,

$$(\pi\rho\dot{n}_0/6) \sum_q D_q{}^3 [\exp\{-\beta(D_q - \bar{D})^2\}] = \dot{m}_{\text{inj}} \qquad (20)$$

where the value of $\dot{m}_{\text{inj}}$ is known. Once n_0 is computed from Eq. (20), the total number of droplets in each diameter class $\dot{n}_q$ is then obtained from Eq. (19). These droplets are spatially distributed with a maximum at $\theta = 135°$ as shown in Fig. 4; thus the value of n_k can be determined as

$$\dot{n}_k = \dot{n}_{qr} = \dot{n}_q \exp\{-\alpha(\theta_r - \bar{\theta})\} \qquad (21)$$

The indices q and r in the preceding equations are related to the subclasses of the droplets categorized by the size and the injection angles, respectively; and θ_r is the spread in the injection angle, whereas α is a characteristic constant for the space distribution. The total number of the classes to be considered for each trajectory k is equal to the total number of the subclass q multiplied by the total number of the subclass r.

In the illustrative example considered in the present paper, the distribution in size is divided into 11 discrete subclasses of 5, 10, 15, 20, 25, 30, 35, 40, 50, 55 μ and the space distribution is spread over the intervals of 105, 115, 125, 135, 145, 155, and 165°. The vaporization calculation thus gives $q \times r = 11 \times 7 = 77$ different trajectories. The total number of particles $\dot{n}_k$ to be used in the computation of Eq. (16) in the 20 μ subclass with injection angle of $\theta = 145°$, for example, is approximately 9.1×10^4 for 0.1 g/sec injection, whereas $\dot{n}_k$ in the 30 μ subclass with $\theta = 135°$ is approximately 4.5×10^5. Typical results of computed vaporization histories for 30 μ droplets are given in Table 2. It is interesting to note that the water is completely distilled from the solution droplet in about 0.5 msec for a 40% NaOH aqueous solution, whereas the NaOH vaporization is completed in about 10 msec. (These values change considerably with injection angle, solution concentration, freestream pressure, and boundary-layer temperature distributions).

The seeding effect in the boundary layer was then studied using the nonequilibrium stream tube, Eq. (13), with the amount of water and NaOH vapor added to each of five stream

Table 2 Typical vaporization process for 30 μ droplet

$D_0 = 30\ \mu$		At t msec 0.5	1.0	1.5	2.0
$\theta = 125°$	D, μ	23.6	18.5	14.7	12.5
	V, m/sec	155.	1095.	2925.	3876.
	X, cm	122.	148.	249.	422.
	y, cm	0.204	0.409	0.613	0.816
$\theta = 135°$	D, μ	24.3	19.8	18.4	16.4
	V	126.	785.	2216.	3313.
	X	122.	141.	215.	356.
	y	0.176	0.353	0.529	0.705
$\theta = 145°$	D, μ	24.6	19.8	17.5	16.2
	V	97.	544.	1586.	2685.
	X	121.	135.	186.	295.
	y	0.143	0.286	0.429	9.572

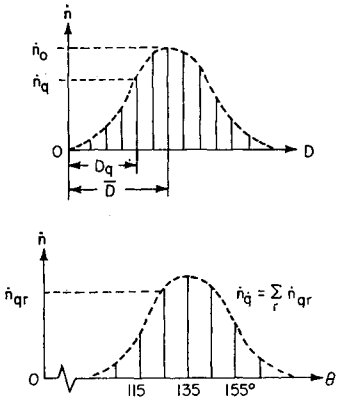

Fig. 4 Space and size distributions of spray droplets.

tubes according to the results of calculation utilizing Eq. (17). A computer program was developed to solve the heat and mass transfer equations together with the chemical rate processes in the boundary layer.

6. Discussion

Typical results of the important species distributions are presented in Figs. 5–8. These illustrations summarize the physical nature of the boundary-layer seeding which is disclosed by the present study.

The initial mass fraction profiles for water and NaOH vapor corresponding to the injection mass flow rates of 0.1 and 1.0 g/sec are shown in Fig. 5. It is seen that the seedant vaporization rate increases and results in a peak at the vicinity of $y/\delta \simeq 0.2$ as the injectant cross flow passes through the peak temperature region in the boundary layer. The decrease in vapor concentration at the edge of the boundary layer results from the reduced heat-transfer rate and the dilution caused by the entrained cool air. The radial distributions of the electrons at the various downstream locations also exhibit the similar peaks along the peak temperature in the boundary layer.

Figures 6 and 7 show typical transverse variations of peak ion mass fractions for the 0.1 and 1.0 g/sec seedant injection rates. It is noted that for negative ions, the peak ion density does not necessarily correspond to the peak boundary-layer temperature. The results show an overshoot in sodium ion density and large deviation from equilibrium. It is also noted that the NO^+ density is somewhat decreased from the corresponding clean air value as a result of charge exchange with sodium. The peak in the H_3O^+ ion density results from the initial chemi-ionization followed by rapid charge exchange with sodium which leads to dissociation of H_3O^+.

As shown in Figs. 6 and 7, the dominant negative ion in the boundary layer is OH^-. The rather high concentration of negative ions relative to positive ions results from the use of faster two-body dissociative attachment rate processes.

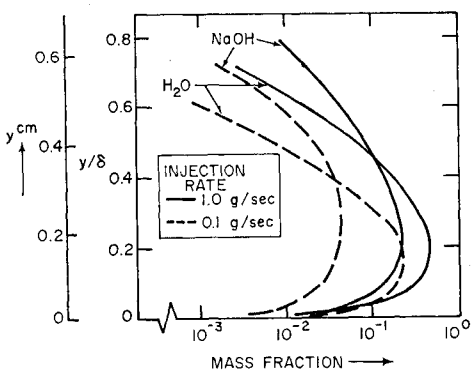

Fig. 5 Initial profiles for NaOH and water vapor.

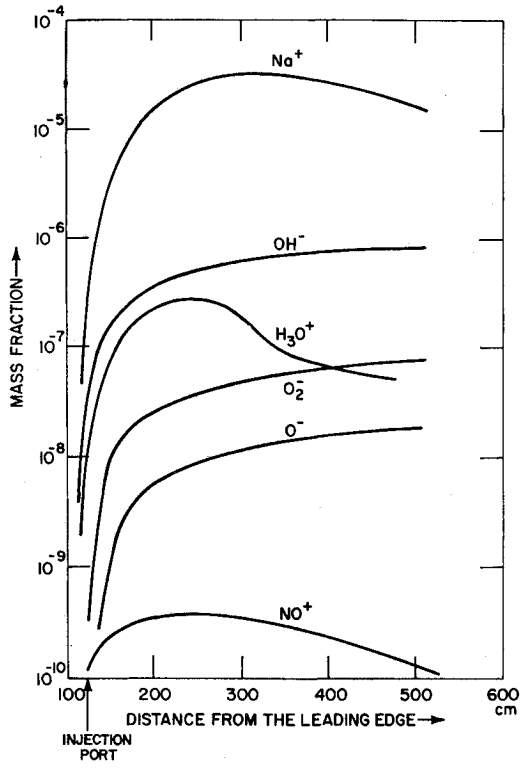

Fig. 6 Boundary-layer charged species peak concentration (0.1 g/sec injection).

However, the effect of attachment of electrons to OH is not sufficient to nullify the effect of seeding. It is further noted that the sodium ion density is not directly proportional to the mass injection rate. This reflects the effect of heterogeneous flowfield coupling processes on the final ion chemistry.

The peak electron density in the boundary layer is shown in Fig. 8. Approximately 4 orders of magnitude increase in electron density over clean air results from the seeding. Increasing the flow rate from 0.1 to 1.0 g/sec only produces a factor of 4 increase in electron density. The substantial seeding results from ionization of Na vapor, which in turn is produced both by the dissociation of NaOH and by the reaction of atomic hydrogen with NaOH. At the peak temperature in the boundary layer, significant amounts of atomic H are formed in the chain branching reactions resulting from dissociation of water vapor. Specifically, the important chemical processes are identified as

$$\mathrm{NaOH} + (M) \rightarrow \mathrm{Na} + \mathrm{OH} + (M)$$

$$\text{and} \begin{cases} \mathrm{H_2O} + (M) \rightarrow \mathrm{H} + \mathrm{OH} + (M) \\ \mathrm{NaOH} + \mathrm{H} \rightarrow \mathrm{Na} + \mathrm{H_2O} \end{cases}$$

where $(M) = \mathrm{O_2}, \mathrm{N_2}$

followed by the ionization reaction

$$\mathrm{Na} + (M) \rightarrow \mathrm{Na^+} + \mathrm{e^-} + (M)$$

It should be pointed out that the reduction of the free electron density in the plasma by the injected droplets themselves[27] has not been considered in detail in this study. However, because of the very large concentration of salt in the solution and the small mass flow of injectant, it is estimated by procedures outlined in Ref. 28 that the droplet density ($\sim 10^6$) is so much smaller than the sodium ion density ($\sim 10^{11}$) that the attachment of electrons to the droplets is insignificant in reducing the free electron density. With more dilute solutions and higher mass flows, this effect could be a problem in the use of solutions for boundary-layer seeding and in fact could result in quenching instead of seeding.

It has been assumed also in this study that electron production in the boundary layer is mainly a result of thermal ionization of gaseous sodium atoms and that thermal electrification[13] and other solid surface effects from the salt crystals themselves are less important. As far as the gas phase chemistry is concerned, the thermal ionization is much more effective than chemi-ionization in producing electrons. This observation is in agreement with the results of other investigations on rocket exhaust flows.[29]

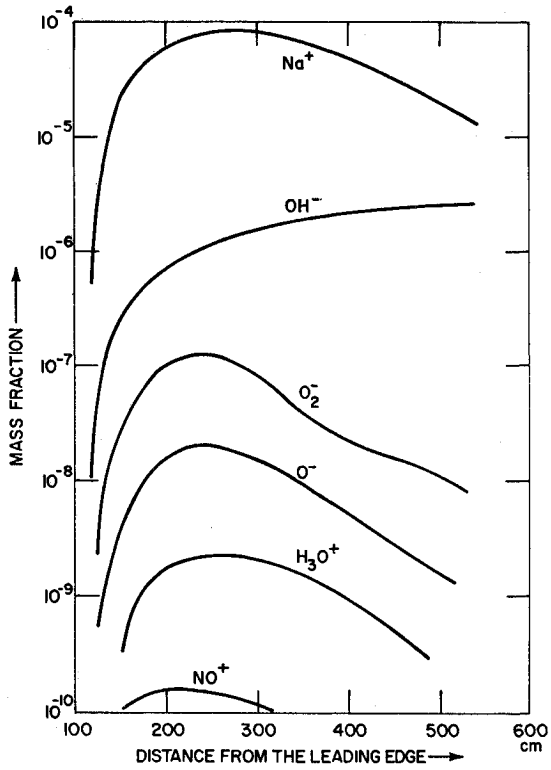

Fig. 7 Boundary-layer charged species peak concentration (1 g/sec injection).

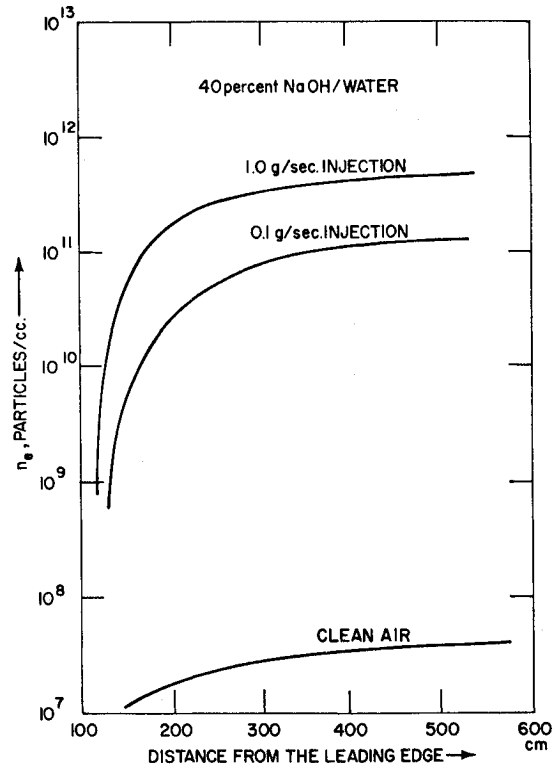

Fig. 8 Boundary-layer peak electron density.

7. Conclusions

The preceding sections have presented an approximate theoretical model and some numerical results for the seeding of a boundary layer by injection of alkali salt solution. Although the entire process is too complicated to allow a completely rigorous fluid mechanical treatment, the mechanism of the seeding and evaporation process has been interpreted on sound physical grounds and the effects of the important parameters have been illustrated. The main observations from the present study are as follows.

1) The important interacting parameters which affect the seeding effectiveness in the boundary-layer ionization are the initial droplet size, the relative magnitude of vaporization time as compared to the residence time, and the ionization kinetics. With regard to the injection mechanism, there exist optimum values for the injection angle and the injection velocity which allow the majority of the droplets to spend most of their residence time in the vicinity of the peak temperature region in the boundary layer.

2) For the seeding of the boundary layer over a flat plate at $x = 1.2$ m with $M \approx 18$, the injection of 0.1 g/sec of 40% NaOH aqueous solution is sufficient to enhance the electron density over that for clean air from 10^7 to 10^{11} particles/cm^3. It is noted that while NaOH and H_2O are only a few percent dissociated within the distance of three meters, the resulting vapor is enough to produce substantial enhancement in electron concentration relative to clean air.

3) Although the effect of pressure and electrolyte concentrations were not systematically varied in the present paper, a careful inspection of the governing equations reveals that the seeding efficiency can be increased somewhat by increasing the ambient pressure and/or concentration of electrolyte. This is mainly due to the effects of increased heat-transfer rate to the droplets, earlier completion of the distillation, and higher rate of vaporization and chemical reactions.

4) Many simplifying assumptions are introduced in the present analysis to make the numerical solution possible. Although it is believed that the accuracy of the results is sufficient to provide relevant characteristics for an overall study of system performance, the results of this study cannot be completely generalized to all situations. The seeding effectiveness depends on the concentration, injection angle, mass flow rate, etc., and additional numerical analysis is required before the correlation of electron enhancement with all these variables can be determined. It is noted that the approximate method developed here can also be applied to the study of the boundary-layer injection of electrophilic fluids[27] and the resulting effect of electron quenching in boundary-layer plasmas.

References

[1] Brogan, T. R., "Ionization in High Temperature Gases," *AIAA Progress in Astronautics and Aeronautics: Ionization in High-Temperature Gases*, Vol. 12, edited by K. E. Shuler, Academic Press, New York, 1963, pp. 319–335.

[2] Foley, R. T. and Vanderslice, T. A., "Seeding of Gases for Magneto-Hydrodynamic Applications," *ARS Journal*, Vol. 32, Oct. 1962, pp. 1573–1576.

[3] Adelberg, M., "Mean Drop Size Resulting from the Injection of a Liquid Jet into a High-Speed Gas Stream," *AIAA Journal*, Vol. 6, No. 6, June 1968, pp. 1143–1147.

[4] Mayer, E., "Theory of Liquid Atomization in High Velocity Gas Streams," *ARS Journal*, Vol. 31, No. 12, Dec. 1961, pp. 1480–1515.

[5] Penner, S. S. and Williams, F. A., eds., *ARS Progress in Astronautics and Rocketry: Detonation and Two-Phase Flow*, Vol. 6, Academic Press, New York, 1962.

[6] Wolfhard, H. G., Glassman, I., and Green, L., Jr., eds., *AIAA Progress in Astronautics and Aeronautics: Heterogeneous Combustion*, Vol. 15, Academic Press, New York, 1964, pp. 667–739.

[7] Edelman, R. and Rosenbaum, H., "Viscous Multicomponent—Multiphase Flow and Application to Axisymmetric Jets of Hydrogen," *AIAA Journal*, Vol. 2, No. 12, Dec. 1964, pp. 2104–2110.

[8] Gayle, J. B., Egger, C. T., and Bransford, J. W., "Freezing of Liquids on Sudden Exposure to Vacuum," *Journal of Spacecraft and Rockets*, Vol. 1, No. 3, June 1964, pp. 323–326.

[9] Pallone, A., Erdos, J., and Moore, J., "Nonequilibrium-Nonsimilar Solutions of the Laminar Boundary Layer Equations," *AIAA Journal*, Vol. 2, No. 10, Oct. 1964, pp. 1706–1713.

[10] Blottner, F. G., "Nonequilibrium Laminar Boundary Layer Flow of Ionized Air," *AIAA Journal*, Vol. 2, No. 11, Nov. 1964, pp. 1921–1927.

[11] Chung, P. M., "Chemically Reacting Nonequilibrium Boundary Layers," *Advances in Heat Transfer*, Vol. 2, Academic Press, New York, 1965, pp. 110–268.

[12] Kavanau, L. L., "Heat Transfer from Spheres to a Rarefied Gas in Subsonic Flow," *Transactions of the ASME*, Vol. 77, July 1955, pp. 617–623.

[13] Soo, S. L., *Fluid Dynamics of Multiphase Systems*, Blaisdell Publishing Co., Waltham, Mass., 1967.

[14] Carlson, D. J. and Hoglund, R. F., "Particle Drag and Heat Transfer in Rocket Nozzles," *AIAA Journal*, Vol. 2, No. 11, Nov. 1964, pp. 1980–1984.

[15] Penner, S. S., *Chemical Reactions in Flow Systems*, Butterworths, London, 1955.

[16] DeRienzo, P. and Wood, A., "Effects of Nonequilibrium on the Hypersonic Laminar Boundary Layer," *Transactions of the 8th Symposium on Ballistic Missile and Space Technology*, Vol. 2, 1963, pp. 36–64.

[17] Wray, K. L., "Chemical Kinetics of High Temperature Air," *ARS Progress in Astronautics and Rocketry: Hypersonic Flow Research*, edited by F. R. Ridell, Academic Press, New York, 1962, pp. 181–204.

[18] Sutton, E. A., "The Chemistry of Electrons in Pure Air Hypersonic Wakes," *AIAA Journal*, Vol. 6, No. 10, Oct. 1968, pp. 1873–1882.

[19] Jensen, D. E. and Kurzius, S. C., "Rate Constants for Calculations on Rocket Exhausts Containing Alkali Metals," TP-149, March 1967, Aerochem Corp., Princeton, N.J.

[20] Jensen, D. E. and Padley, P. J., "Kinetics of Ionization of the Alkali Metals in H_2, O_2, N_2, Flames," *Transactions of the Faraday Society*, Vol. 62, 1966, pp. 2132–2140.

[21] Calcote, H. F., "Relaxation Processes in Plasma," *Proceedings of 3rd Biennial Gas Dynamics Symposium*, Northwestern University Press, Vol. 1, 1960, pp. 36–51.

[22] Branscomb, L. M., "Photo-Detachment Cross Section, Affinity and Structure of the Negative Hydroxyl Ion," *Physical Review*, Vol. 148, 1966, pp. 11–18.

[23] Landon, S. A. and Keck, J. C., "Calculation of Three Body Ionic Recombination Rate," *Journal of Chemical Physics*, Vol. 48, 1968, pp. 374–380.

[24] Gioumousis, G. and Stevenson, D. P., "Reactions of Gaseous Molecule Ions with Gaseous Molecules," *Journal of Chemical Physics*, Vol. 29, 1958, pp. 294–299.

[25] Johnston, H. S., "Bimolecular Collision Dynamics," *Gas Phase Reaction Rate Theory*, Ronald Press, New York, 1966, pp. 101–116.

[26] Hansen, C. F., "Temperature Dependence of the $NO^+ + e$ Dissociative Recombination Rate Coefficient," *The Physics of Fluids*, Vol. 11, April 1968, pp. 904–906.

[27] Evans, J. L., "Reduction of Free Electron Concentration in a Reentry Plasma by Injection of Liquids," *Proceedings of the Third Symposium on the Plasma Sheath*, Air Force Cambridge Research Labs., Vol. III, May 1967, pp. 343–361.

[28] Rosen, G., "Method for the Removal of Free Electrons in a Plasma," *The Physics of Fluids*, Vol. 5, 1962, pp. 737–738.

[29] Pergament, H. S. and Calcote, H. F., "Thermal and Chemi-ionization Processes in After Burning Rocket Exhausts," *Eleventh Symposium (International) on Combustion*, The Combustion Inst., Pittsburgh, Pa., 1967, pp. 597–611.